Applied Catalysis B: Environmental 144 (2014) 223–232

Contents lists available at ScienceDirect

Applied Catalysis B: Environmental

journal homepage: www.elsevier.com/locate/apcatb

Sorption-enhanced synthetic natural gas (SNG) production from syngas: A novel process combining CO methanation, water-gas shift, and CO_2 capture

Vanessa M. Lebarbier[a], Robert A. Dagle[a], Libor Kovarik[a], Karl O. Albrecht[b], Xiaohong Li[a], Liyu Li[a], Charles E. Taylor[c], Xinhe Bao[d], Yong Wang[a,e,*]

[a] Institute for Integrated Catalysis, Pacific Northwest National Laboratory, Richland, WA 99352, United States
[b] Chemical & Biological Process Development, Energy and Environment Directorate, Pacific Northwest National Laboratory, Richland, WA 99352, United States
[c] National Energy Technology Laboratory, Pittsburgh, PA 15236, United States
[d] Dalian Institute of Chemical Physics, Chinese Academy of Sciences, China
[e] Voiland School of Chemical Engineering and Bioengineering, Washington State University, Pullman, WA 99164, United States

ARTICLE INFO

Article history:
Received 7 March 2013
Received in revised form 17 May 2013
Accepted 28 June 2013
Available online 8 July 2013

Keywords:
Methanation
CO_2 sorption
Sorption enhanced reaction
Methanation catalyst
CO_2 sorbent

ABSTRACT

Synthetic natural gas (SNG) production from syngas is under investigation again due to the desire for less dependency from imports and the opportunity for increasing coal utilization and reducing greenhouse gas emission. CO methanation is highly exothermic and substantial heat is liberated which can lead to process thermal imbalance and deactivation of the catalyst. As a result, conversion per pass is limited and substantial syngas recycle is employed in conventional processes. Furthermore, the conversion of syngas to SNG is typically performed at moderate temperatures (275–325 °C) to ensure high CH_4 yields since this reaction is thermodynamically limited. In this study, the effectiveness of a novel integrated process for the SNG production from syngas at high temperature (i.e. 600 °C) was investigated. This integrated process consists of combining a CO methanation nickel-based catalyst with a high temperature CO_2 capture sorbent in a single reactor. Integration with CO_2 separation eliminates the reverse-water-gas shift and the requirement for a separate water-gas shift (WGS) unit. Easing of thermodynamic constraint offers the opportunity of enhancing yield to CH_4 at higher operating temperature (500–700 °C) which also favors methanation kinetics and improves the overall process efficiency due to exploitation of reaction heat at higher temperatures. Furthermore, simultaneous CO_2 capture eliminates greenhouse gas emission. In this work, sorption-enhanced CO methanation was demonstrated using a mixture of a 68% CaO/32% $MgAl_2O_4$ sorbent and a CO methanation catalyst (Ni/Al_2O_3, $Ni/MgAl_2O_4$, or Ni/SiC) utilizing a syngas ratio (H_2/CO) of 1, gas-hour-space velocity (GHSV) of 22,000 h^{-1}, pressure of 1 bar and a temperature of 600 °C. These conditions resulted in ~90% yield to methane, which was maintained until the sorbent became saturated with CO_2. By contrast, without the use of sorbent, equilibrium yield to methane is only 22%. Cyclic stability of the methanation catalyst and durability of the sorbent were also studied in the multiple carbonation–decarbonation cycle studies proving the potential of this integrated process in a practical application.

1. Introduction

Fossil fuels, primarily petroleum, coal and natural gas, are the major sources of energy worldwide. Natural gas is the world's fastest-growing fossil fuel, with consumption increasing at an average rate of 1.6 percent per year since 2008 [1]. Increasing demand and price volatility of natural gas have made the production of synthetic natural gas (SNG) from carbon sources (coal, petcoke, biomass or municipal solid waste) attractive in some regions of the world. SNG production from coal is especially important in China where natural gas consumption has increased from 15 bcm in 1980 to 110 bcm in 2010 [2]. Large state owned companies have shown great interest in coal-based SNG production since coal is highly abundant in China and natural gas from coal is considered as the most promising low greenhouse gas emission option in China [2]. Gasification of coal, petcoke, biomass or municipal solid waste results in the production of a syngas containing mainly H_2 and CO.

* Corresponding author at: Institute for Integrated Catalysis, Pacific Northwest National Laboratory, Richland, WA 99352, United States.
E-mail address: yongwang@pnnl.gov (Y. Wang).

0926-3373/$ – see front matter © 2013 Elsevier B.V. All rights reserved.
http://dx.doi.org/10.1016/j.apcatb.2013.06.034

H_2/CO ratio of the syngas can be adjusted by water-gas shift reaction, and this syngas can be then converted to methane, the major component of natural gas, through CO methanation.

Several methanation processes have been developed comprising fixed bed and fluidized bed methanation reactors. Fluidized bed methanation allows for isothermal operation, useful due to the high exothermicity of the reaction. For a fixed bed process, heat of reaction usually needs to be removed by a combination of intermediate reactors and gas cooling [3]. Catalysts for the fluidized beds have to be attrition resistant while for fixed bed operation, active metal sintering due to higher reaction temperatures can be problematic. Most of the known methanation processes utilize fixed bed reactors due to their relative simplicity.

The Lurgi's coal gasification process is a well known commercial technology for the production of synthetic natural gas, developed in the 1960s and 1970s [3]. Lurgi developed a methanation unit including two adiabatic fixed bed reactors with internal gas recycling. The first reactor bed was operated from 300 °C for the inlet temperature to 450 °C for the outlet temperature. The second reactor bed was operated at a lower temperature, from 260 °C for the inlet temperature to 315 °C for the outlet temperature. The only commercial plant for SNG production from coal is based on Lurgi's process and is located in North Dakota (USA). It consists of 14 Lurgi Mark IV fixed bed gasifiers followed by a shift conversion unit, a Rectisol unit for CO_2 and sulphur removal, and a methanation unit. The TopsØe's Recycle Energy Efficient Methanation Process (TREMP process) is also based on a fixed bed methanation reactor unit [3,5]. The TREMP process is a heat recovery concept which produces high pressure superheated steam. The temperature in the first reactor ranges from 350 °C for the inlet of the bed to 700 °C for the outlet of the bed and the pressure up to 3 MPa. To decrease the unwanted high temperature, steam is introduced through a super heater unit producing high pressure superheated steam. This technology requires catalysts with high temperature stability. Haldor TopsØe has developed catalysts such as MCM-2X (nickel-based catalyst) for CO methanation at 300–700 °C. However, the high temperature stability of MCM-2X is questionable. A study from Rostrup-Nielsen showed that the production of methane decreased progressively with time due to sintering of Ni particles [6]. There is thus a need for more robust catalysts when operating under severe temperature conditions. The Conoco/British Gas Corporation (BGC) process, similarly to the Lurgi and the TREMP processes, consists of separate methanation, WGS and CO_2 capture units [3]. The HICOM process developed by the BGC is based on a slightly different concept as the methanation and the WGS units are combined in one [3].

In this report we describe an integrated process for the production of synthetic natural gas. This process combines CO methanation, WGS and CO_2 capture in one single reactor. This suppresses the reverse water-gas-shift reaction, increases the CO conversion to CH_4, and eliminates the need for a separate WGS unit. This concept requires the use of a sorbent for CO_2 capture with sufficient CO_2 uptake kinetics that can be combined with CO methanation catalyst. Note that a similar concept has been successfully demonstrated for sorption-enhanced H_2 production process involving hydrocarbon reforming, WGS and CO_2 separation [4]. For conventional CO methanation, being thermodynamically limited, the optimal temperature to obtain high selectivity to CH_4 (i.e. >90%) is approximately 300 °C. Combined with effective CO_2 sorption, selectivity to CH_4 is not limited by thermodynamic equilibrium even by operating at higher temperatures (e.g. 500–600 °C). High temperature operation also improves the overall process efficiency by exploiting high temperature reaction heat and enhances the methanation kinetics. Furthermore, due to relaxed thermodynamics, an integrated process could potentially operate at much lower pressure, as compared to conventional CO methanation, further improving process efficiency. In addition, simultaneous CO_2 capture would eliminate greenhouse gas emission without need for additional CO_2 capture technology. Upon sorbent regeneration, desorption would provide a concentrated CO_2 source for subsequent sequestration and utilization.

CO methanation catalysts are typically Ni-based and supported on an alumina-type support [6–9]. $MgAl_2O_4$ has been reported as a more stable support than Al_2O_3 for the dry reforming of methane at high temperature (i.e. 600–800 °C) [10]. Thus, Ni/$MgAl_2O_4$ catalysts could be more suitable than Ni/Al_2O_3 catalysts for CO methanation at high temperature. SiC is well known for its excellent thermal stability and high thermal conductivity. These properties make SiC an attractive support for exothermic reactions. Ni/SiC catalysts are thus potential candidates as well, and have been evaluated in other studies [11–13]. For high temperature CO_2 adsorption, CaO-based sorbents are typically used [14,15], based on the reversible chemical reaction:

$$CaO_{(s)} + CO_{(g)} \rightarrow CaCO_{3(s)} \text{ carbonation}$$

$$CaCO_{3(s)} \rightarrow CaO_{(s)} + CO_{2(g)} \text{ decarbonation}$$

The CaO-based sorbent usually suffers from rapid loss of CO_2 sorption capacity over many carbonation/decarbonation cycles due to severe sintering [16]. Recently, we found that the sintering effect can be mitigated by mixing CaO precursors with $MgAl_2O_4$ spinel nanoparticles [15], and a CaO/$MgAl_2O_4$ sorbent was thus developed which exhibits an improved durability compared to a natural dolomite.

The objective of this study was to investigate the feasibility of an integrated process with suitable CO_2 sorbents and methanation catalysts. We first performed the CO methanation equilibrium calculations in absence and presence of sorbent to show the thermodynamics benefit of adding CO_2 sorption. Then CaO/$MgAl_2O_4$ sorbent was evaluated for CO_2 sorption at 600 °C and desorption at 800 °C, followed by the proof-of-concept studies for the combined reaction-sorbent integrated process with multiple CO_2 sorption–desorption cycles. Finally, the nickel-based catalysts (i.e. Ni/Al_2O_3, Ni/$MgAl_2O_4$ and Ni/SiC) were evaluated for CO methanation without sorbent addition and characterized using transmission electron microscope (TEM) and X-ray diffraction (XRD)

2. Experimental

2.1. Catalysts and sorbent preparation

A series of supported Ni catalysts were prepared by incipient wetness impregnation of Al_2O_3 (Sasol, Puralox TH100/150), SiC (American Elements, Si-C-02-NP.040N) and $MgAl_2O_4$ (Sasol Puralox 30/140) with a solution of Ni nitrate hexahydrate (Sigma–Aldrich 99%) dissolved in acetone. After impregnation, the catalysts were dried at 110 °C for 8 h and calcined under static air at 350 °C for 3 h. The Ni loading was 20 wt% for all three catalysts which are denoted as 20%Ni/Al_2O_3, 20%Ni/SiC and 20%Ni/$MgAl_2O_4$. A 68%CaO/$MgAl_2O_4$ sorbent was synthesized according to the method described in Ref. [15]. The sorbent was synthesized by overnight ball-millings of a 2-propanol slurry containing $Ca(CH_3COO)_2$ and $MgAl_2O_4$ particles, followed by drying and calcining in static air at 800 °C for 2 h. The sorbent contains 68 wt% CaO and 32 wt% $MgAl_2O_4$. Note that the term "spent" refers to the catalysts exposed to the reaction conditions.

2.2. BET surface area

Nitrogen adsorption was measured at 77 K with an automatic adsorptiometer (Micromeritics ASAP 2000). Samples were pretreated at 150 °C for 12 h under vacuum. The surface areas were

determined from adsorption values for five relative pressures (P/P_0) ranging from 0.05 to 0.2 using the BET method. The pore volumes were determined from the total amount of N_2 adsorbed between $P/P_0 = 0.05$ and $P/P_0 = 0.98$.

2.3. X-ray diffraction (XRD)

X-ray powder diffraction spectra were recorded using a Philips X'pert MPD (Model PW3040/00) diffractometer with copper anode ($K\alpha_1 = 0.15405$ nm) and a scanning rate of 0.002° per second between $2\theta = 10°$ and 70°. The diffraction patterns were analyzed using Jade 5 (Materials Data Inc., Livermore, CA) and the Powder Diffraction File database (International Center for Diffraction Data, Newtown Square, PA). Particle sizes of the samples were determined from the XRD patterns using the Debye–Sherrer relation ($d = 0.89\lambda/B\cos\theta$, where λ is the wavelength of Cu Kα radiation, B is the calibrated half-width of the peak in radians, and θ is the diffraction angle of a crystal face). The particle sizes were determined from the peaks located at $2\theta = 52°$ and 53.9°, respectively for Ni° and CaO.

2.4. Transmission electron microscopy (TEM)

Transmission electron microscopy (TEM) measurements were conducted with a FEI Titan 80-300 operated at 300 kV. All images were digitally recorded using a charge-coupled device (CCD) camera and were analyzed using Gatan Digital Micrograph. TEM images were collected from at least five different locations on the grid. In general, the TEM sample preparation involved mounting of powder samples on copper grids covered with lacey carbon support films and immediate loading them into the TEM airlock to minimize an exposure to atmospheric O_2.

2.5. Temperature programmed oxidation (TPO)–thermogravimetric analysis (TGA)

The TPO–TGA experiments were conducted with a Netzsch 409C Thermogravimetric Analyzer to determine the amount of coke present in the spent samples. A 1% O_2/Ar gas mixture was passed through the sample starting from 20 °C and heating up to 900 °C with a ramp of 10 °C/min.

2.6. Sorbent performance measurements

The performance of the 68% $CaO/MgAl_2O_4$ sorbent was first tested using a 7 mm inner diameter fixed-bed reactor connected to an Agilent Micro-GC equipped with a Molsieve and a Poraplot U column. Carbonation was carried out at 600 °C by flowing 23% CO_2/N_2 (4.7 sccm CO_2 + 15.6 sccm N_2), followed by a decarbonation at 800 °C under 50 sccm N_2 for 1 h. In some of the tests, to test the regenerability of the sorbent, we have carried out a carbonation–decarbonation cycle with either H_2O addition to the feed during the carbonation step or H_2O treatment before carbonation. For the tests where H_2O was added to the feed during the carbonation test, the gas mixture was composted of 19% CO_2 (4.7 sccm), 64% N_2 (16.7 sccm) and 17% H_2O (4.2 sccm). When H_2O treatment was done before carbonation, a mixture of 17% H_2O in N_2 (H_2O = 4.2 sccm) was first flown at 600 °C for 1 h then the catalyst was reduced at the same temperature by flowing 10%H_2/N_2 for 1 h. Each carbonation step conducted with 0.35 g of sorbent lasted 0.5 h. For the integrated tests, 0.7 g of sorbent was used and the carbonation step lasted 1 h. CO_2 sorption capacity is defined as the amount of CO_2 adsorbed (CO_2 in grams) per gram of sorbent. The reactor was connected to a micro-GC that would detect CO_2 when the sorbent reaches its CO_2 sorption capacity. The time it takes before CO_2 detection from the micro-GC was recorded. From this time and the CO_2 flow, the amount of CO_2 adsorbed by the sorbent was determined.

2.7. CO methanation equilibrium calculations in the absence or presence of sorbent

The concentrations of gaseous components at thermodynamic equilibrium were determined by simultaneously solving the appropriate equilibrium expressions similar to the method described by Thompson [17]. The equilibrium calculations were based on a closed isothermal system charged with 0.48 mol of CO, 0.48 mol of H_2 and 0.04 mol of N_2. CO and H_2 were allowed to react via the CO methanation reaction (Reaction (1)) and water-gas shift reaction (Reaction (2)) in order to come to an equilibrium mixture of CH_4, H_2O, CO, CO_2 and H_2. N_2 was considered to be inert. Two systems were considered. First, a system without CaO sorbent was considered where only reactions (1) and (2) were employed. This case is considered to be only for reaction. Secondly, a system with CaO sorbent was considered in which reactions (1) and (2) were active in addition the specific sorption of CO_2 from the system by the CaO via the formation of $CaCO_3$ (Reaction (3)). The latter is considered for the integrated reaction-sorption system. The equilibrium constants for reactions (1) and (2) as well as reaction (3) were from published sources [17,18]. The reactions considered are as follows:

$$CO + 3H_2 \leftrightarrow H_2O + CH_4 \quad (1)$$

$$CO + H_2O \leftrightarrow CO_2 + H_2 \quad (2)$$

$$CaO + CO_2 \leftrightarrow CaCO_3 \quad (3)$$

2.8. Reactivity measurements

Catalytic activity tests were conducted in a 7 mm inner diameter fixed-bed quartz reactor at ambient pressure. Two K-type thermocouples were placed in the reactor for the measurement of inlet and catalyst bed temperatures. Catalysts were reduced at 600 °C for 2 h, using 10% H_2/N_2 gas mixture, prior to the test. The integrated tests were performed in the presence of 0.1 g of catalyst and 0.7 g of sorbent. For the integrated tests, multiples cycles of carbonation–decarbonation were conducted. The carbonation was conducted under CO methanation reaction conditions by flowing a mixture of H_2, CO, N_2 and H_2O ($H_2/CO/N_2/H_2O$ = 38.4/38.4/3.2/20) at 600 °C for 1 h, P = 1 bar, and GHSV = 22,000 h^{-1}. The decarbonation was carried out at 800 °C, by flowing 50 sccm of N_2 for 1 h. Stability test measurements for the CO methanation reaction were then conducted by loading the reactor with 100 mg of catalyst diluted with 3 g of SiC in order to keep the catalyst bed isothermal. These measurements were conducted at 500 °C, P = 1 bar, GHSV = 87,000 h^{-1} and a gas mixture containing H_2 (48%), CO (48%) and N_2 (4%). Note that the CH_4 and CO_2 selectivites were calculated based on the gas phase composition only and do not include the solids products.

3. Results and discussion

3.1. Thermodynamics of the CO methanation reaction in the absence or presence of CO_2 sorption

The CO methanation reaction is a thermodynamic equilibrium limited process. Calculating chemical equilibrium using Eqs. (1) and (2) provide the thermodynamic composition for the system assuming only these reactions occurring. As shown in Fig. 1, for a molar feed composition of H_2/CO = 1, CO conversion decreases as the reaction temperatures increases. For example, CO conversion decreases from 97% to 52% when temperature increases from

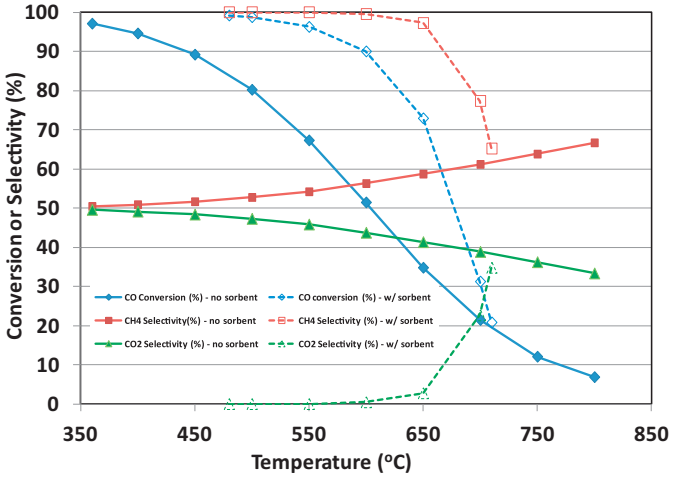

Fig. 1. Equilibrium CO conversion, CH_4 selectivity, and CO_2 selectivity as a function of temperature, calculated either in the absence or presence of sorbent (P = 1 atm, molar composition: H_2 = 48%, CO = 48%, N_2 = 4%).

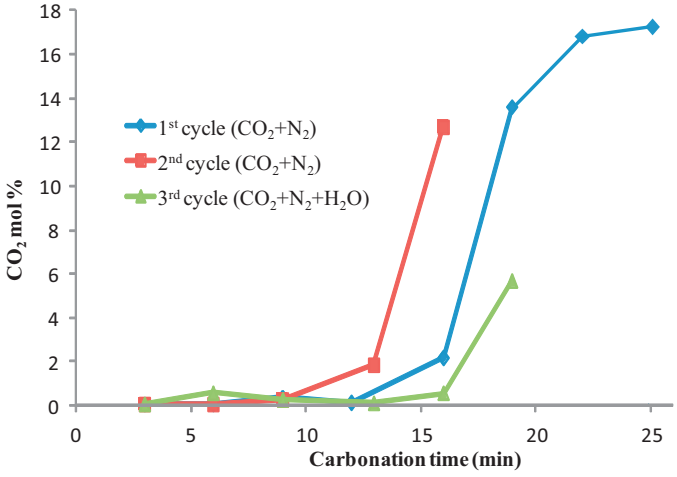

Fig. 2. Evolution of the CO_2 mol% detected from the micro-GC as a function of the carbonation time. T = 600 °C, 23% CO_2/N_2 (i.e. 4.7 sccm CO_2, 15.6 sccm N_2), sorbent = 0.35 g. For the 3rd cycle, H_2O was added to the feed (19% CO_2 = 4.7 sccm, 64% N_2 = 16.7 sccm and 17% H_2O = 4.2 sccm).

350 °C to 600 °C. Equilibrium selectivities for both CO_2 and CH_4 are shown in Fig. 1 as well. At 350 °C the selectivity to CO_2 and CH_4 are each approximately 50%. With increasing temperature, selectivity to CO_2 decreases as the water-gas shift reaction (Eq. (2)) is disfavored. At 600 °C, equilibrium selectivities to methane and CO_2 are approximately 56% and 44%, respectively.

Thermodynamic benefit for adding CO_2 sorption to the system is illustrated by integrating all three reactions; CO methanation (Eq. (1)), water-gas shift (Eq. (2)), and CO_2 sorption (Eq. (3)). By incorporating Eq. (3) to the reaction system, CO_2 is selectively removed by CaO adsorption, forming $CaCO_3$, and water-gas shift reaction is highly favored. As shown in Fig. 1, even at 600 °C, CO conversion is still relatively high at approximately 90%. Also at 600 °C, selectivities to CH_4 and CO_2 are approximately 99.5% and 0.5%, respectively. Such high equilibrium selectivity to methane is highly desired for this process. As the temperature further increases from 600 °C to 700 °C, selectivity to CH_4 quickly decreases and approaches the value when no CO_2 sorption was included in the equilibrium calculations, due to the fact that CaO carbonation to form $CaCO_3$ (Eq. (3)) is disfavored at such a high temperature. Hence, operating at 600 °C seems to be an appropriate condition to obtain high yield of methane. This is also an optimal temperature for the CaO-based sorbents to perform well [14,15,19]. Before experimental proof-of-concept demonstration of this novel process, we have thus examined the performance and properties of the 68% $CaO/MgAl_2O_4$ for CO_2 sorption at 600 °C.

3.2. CO_2 sorbent performance results and characterization

Three carbonation–decarbonation cycles were conducted in order to evaluate the performance of the 68%$CaO/MgAl_2O_4$ sorbent at 600 °C. Fig. 2 depicts the amount of CO_2 detected from the gas phase as a function of the time on stream during the carbonation step for each cycle. For the first cycle, CO_2 was not detected for the first 12 min indicating that CO_2 was adsorbed during this time. After 12 min, CO_2 was detected from the gas phase signifying that the sorbent had reached its CO_2 sorption capacity. The CO_2 sorption capacity of the sorbent for this first cycle was thus estimated to be ~32 wt%. After that, the sorbent was heated to 800 °C under N_2 flow and held for 1 h at this temperature for total decarbonation. Then, to examine the durability of the sorbent, a second cycle of carbonation–decarbonation was conducted under the same conditions. As can be seen from Fig. 2, CO_2 was detected from the gas phase after only 9 min time-on-stream. This shows that the CO_2 sorption capacity of the sorbent decreased and that it deactivated to some extent. The CO_2 sorption capacity of the sorbent for this second cycle was only ~24 wt%. The decrease in activity of CaO sorbents after multiple cycles has been reported [20–22]. Abanades and Alvarez [21] have attributed the decrease in activity, for an untreated limestone (i.e. CaO), to sintering as the number of carbonation–decarbonation cycles increase. Anthony and coworkers [19,20] have shown that CaO sorbent can be reactivated by a steam treatment under pressure. To test the regenerability of the 68% $CaO/MgAl_2O_4$ sorbent, we have thus carried out a third carbonation–decarbonation cycle with either H_2O addition to the feed during the carbonation step or H_2O treatment before carbonation. Fig. 2 presents the results obtained for the third cycle when H_2O (17 mol%) was added to the feed during the carbonation step. CO_2 was not detected during the first 13 min indicating that it was reactivated in the presence of H_2O. Indeed, the CO_2 sorbent capacity for the third cycle was ~34 wt% and quite similar to the one observed for the first cycle. Note that the same results were obtained when H_2O treatment was conducted before the carbonation.

Fig. 3 shows the XRD patterns recorded for the 68% $CaO/MgAl_2O_4$ sorbent, before any carbonation–decarbonation cycle (labeled as "fresh"), after the 1st carbonation and after each carbonation–decarbonation cycle, between 2θ = 15° and 70°. As expected, the XRD pattern recorded for the fresh sorbent presents mainly peaks characteristic of CaO and $MgAl_2O_4$. Small peaks due to $Ca(OH)_2$ and $CaCO_3$ were also observed which can be attributed to the exposure of the sorbent to the atmosphere. The XRD pattern obtained after the 1st carbonation (i.e. before decarbonation) shows peaks attributed to $CaCO_3$, due to the transformation $CaO \rightarrow CaCO_3$. Peaks due to CaO are observed as well, suggesting that during the carbonation CaO was not completely utilized. This is consistent with our previous study showing a 63% utilization of CaO with a similar 68% $CaO/MgAl_2O_4$ sorbent [15]. The subsequent decarbonation step of the sorbent leads to a complete transformation of $CaCO_3$ to CaO since no peaks characteristic of the carbonate species are seen from the XRD pattern (see Fig. 3). Note that very small peaks due to $Ca(OH)_2$ were observed which are likely due to the exposure of the sorbent to the atmosphere (on subsequent handling). The XRD patterns recorded after the 2nd carbonation/decarbonation cycle are similar to the one recorded after the first carbonation/decarbonation cycle. The XRD pattern obtained after the third carbonation–decarbonation cycle shows the intense peaks which

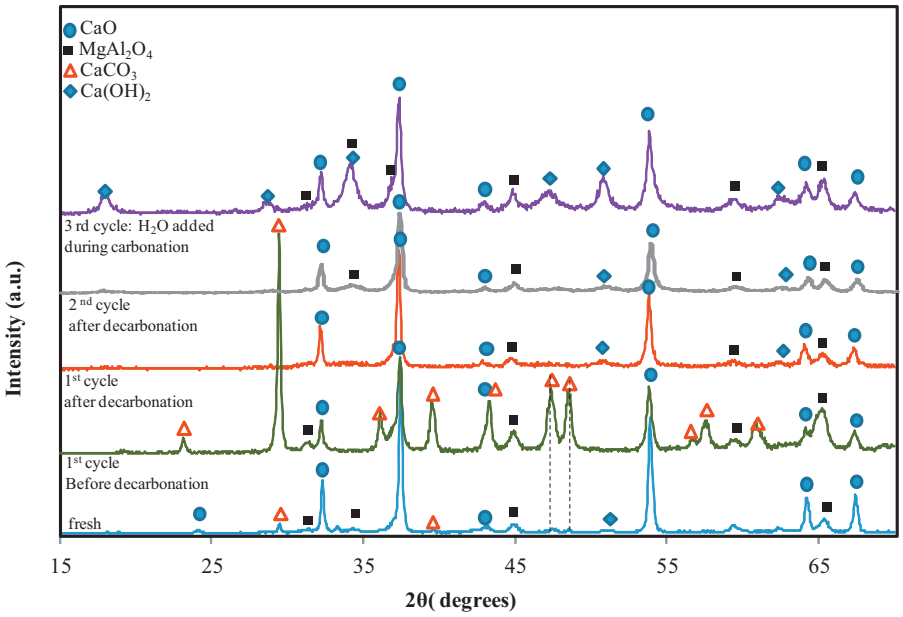

Fig. 3. XRD patterns recorded for the 68% $CaO/MgAl_2O_4$ sorbent before any carbonation–decarbonation cycle labeled as "fresh", after carbonation for the 1st cycle and after decarbonation for each cycle.

are attributed to CaO and $Ca(OH)_2$ as well as peaks due to $MgAl_2O_4$. The addition of H_2O to the feed during the third carbonation cycle led to the (partial) transformation of CaO to $Ca(OH)_2$. After the third carbonation/decarbonation cycle, the CaO crystallite size was equal to 26 nm which was lower than the CaO crystallite size after the first carbonation/decarbonation cycle (i.e. 36 nm). Hence, addition of H_2O to the feed prevented the sintering of CaO and resulted in smaller CaO particles. These results are in agreement with those obtained by Hughes et al. [19], who have shown that hydration of limestone leads to the formation of cracks in the lime particles and thus an increase of the surface area and the pore volume. A separate experiment where the H_2O treatment was conducted before the third carbonation/decarbonation cycle has also shown that the sorbent was also efficiently regenerated upon hydration. These results suggest that for multiple carbonation–decarbonation cycles, deactivation of the 68% $CaO/MgAl_2O_4$ sorbent could be prevented by adding H_2O to the feed during carbonation. This can be readily practiced since the water content is between 2% and 30% in a coal-derived syngas depending on the gasifier and type of coal [23].

3.3. Integrated CO methanation, WGS, and CO_2 capture

3.3.1. Integrated sorption-reaction

Proof-of-concept studies for integrating CO methanation with CO_2 capture were performed using 20%Ni/SiC. SiC was expected to be a more appropriate support for exothermic reactions due to its superior thermal stability and high thermal conductivity. These integrated tests were performed at 600 °C with the 68% $CaO/MgAl_2O_4$ sorbent mixed with the catalyst. For reasons described above, H_2O was included in the feed such that the total feed composition was comprised of 38.4% H_2, 38.4% CO, 20% H_2O, and 3.2% N_2. A syngas ratio of 1 was chosen to reflect the H_2/CO ratio of the gas mixture coming out of the gasifier even though lower ratios are likely to favor coking of the catalyst. Integrated testing results are shown as a function of time-on-stream in Fig. 4. CO conversion of >95% and selectivity to methane of >98% were achieved and maintained for at least 20 min TOS. Thus, the CO_2 formed was efficiently adsorbed by CaO and the mixed sorbent-catalyst system was efficient under these conditions to convert CO to CH_4. After approximately 25 min TOS, the sorbent became saturated with CO_2 and it was calculated that the sorbent reached a CO_2 capacity of ~34 wt%, which approximates that as reported previously in the case of CO_2 capture alone [15]. Upon reaching CO_2 sorption capacity, CO conversion and CH_4 selectivity dropped to 31% and 58%, respectively, approaching the equilibrium values. Fig. 5 further illustrates these results in terms of CH_4 yield. Note that the CH_4 yield was calculated from the CO conversion and the gas phase CH_4 selectivity. A significantly high CH_4 yield (92%) was observed for the integrated test, as compared to the methane yield of 18% under reaction-only conditions (without CO_2 sorption) which is close to an equilibrium yield of ~22%. These results highlight the performance benefits realized when the kinetics of CO_2 uptake and methanation are properly matched.

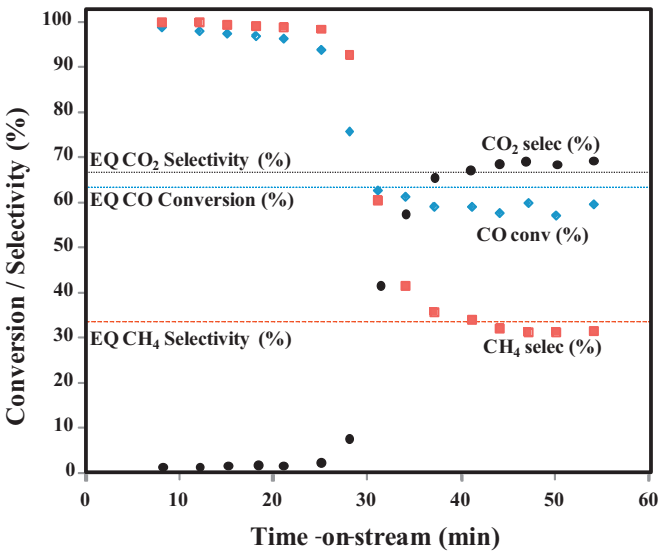

Fig. 4. Integrated sorption-reaction demonstration [T = 600 °C, P = 1 atm GHSV = 22,000 h^{-1}, molar feed composition: H_2 = 38.4%, CO = 38.4%, H_2O = 20%, N_2 = 3.2%; catalyst = 0.1 g (20%Ni/SiC), sorbent = 0.7 g, SiC = 3.0 g (diluent)].

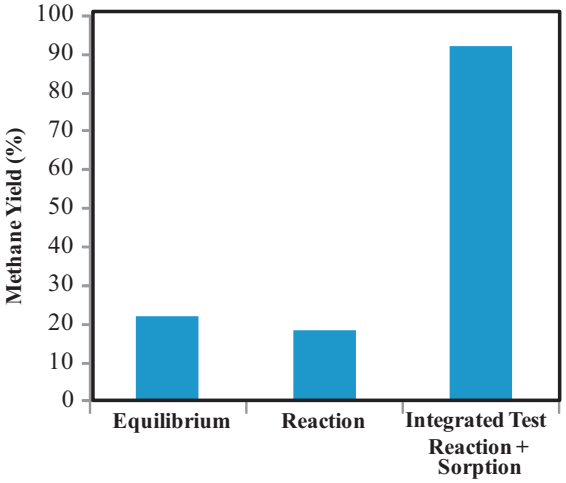

Fig. 5. Methane yield comparison between integrated process, and reaction-only testing results and equilibrium (T = 600 °C, P = 1 atm, feed composition: H_2 = 38.4%, CO = 38.4%, H_2O = 20%, N_2 = 3.2%).

3.4. Cycling experiments

The cyclic stability of both catalyst and sorbent for the integrated test was evaluted in the multiple carbonation/decarbonation cycle studies. The carbonation was conducted under CO methanation reaction conditions at 600 °C for 1 h. The decarbonation was carried out at 800 °C, by flowing 50 sccm of N_2 for 1 h. The 20%Ni/SiC catalyst was found to be unsuitable for cyclic studies because not only the initial CO conversion after the first carbonation/decarbonation cycle reduced significantly (~28%) but it also deactivated during the second carbonation cycle as shown in Fig. 6. The deactivation during cycle 2 is attributed to the formation of amorphous carbon (see TEM image Fig. 12). We have thus conducted these multiple carbonation/decarbonation cycles with the 20%Ni/Al_2O_3 catalyst. Fig. 7 presents the CO conversion and CH_4 selectivity obtained for multiple carbonation–decarbonation cycles over the 20%Ni/Al_2O_3 catalyst. The CO conversion decreases from 90% for the first cycle to 65% for the fifth cycle indicating that the catalyst suffers from deactivation. Note that the CH_4 selectivity was stable and equal to about 99% for each cycle indicating no significant deactivation of the

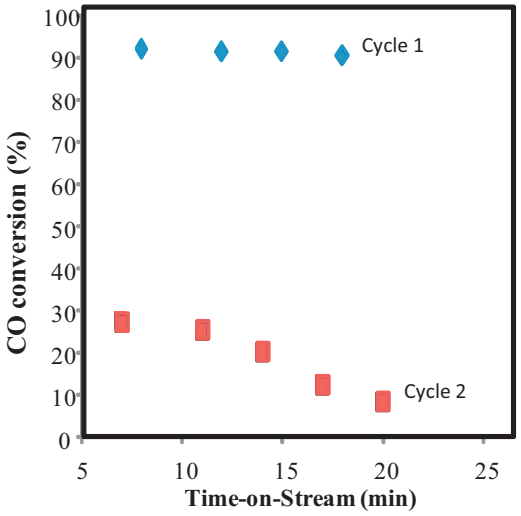

Fig. 6. CO conversion as a function of the time-on-stream for the first two cycles using the 20%Ni/SiC catalyst and 68%CaO/$MgAl_2O_4$ sorbent [T = 600 °C, P = 1 atm, GHSV = 22,000 h^{-1}, molar feed composition: H_2 = 38.4%, CO = 38.4%, H_2O = 20%, N_2 = 3.2%; catalyst = 0.1 g, sorbent = 0.7 g].

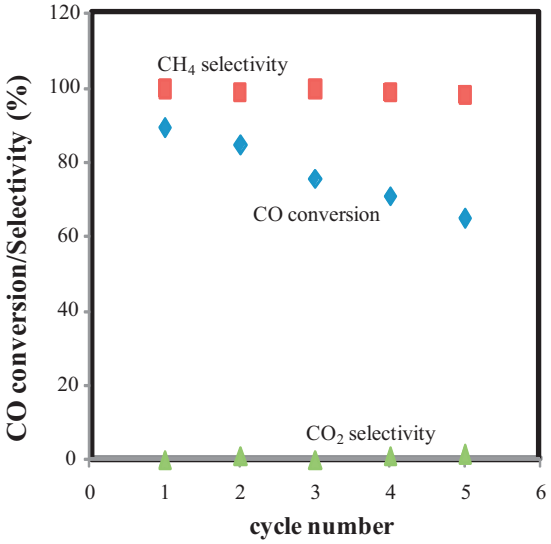

Fig. 7. CO conversion, CH_4 and CO_2 selectivities for each carbonation/decarbonation cycle, for the 20%Ni/Al_2O_3 catalyst and 68%CaO/$MgAl_2O_4$ sorbent [T = 600 °C, P = 1 atm, GHSV = 22,000h^{-1}, molar feed composition: H_2 = 38.4%, CO = 38.4%, H_2O = 20%, N_2 = 3.2%; catalyst = 0.1 g, sorbent = 0.7 g].

sorbent. Since both 20%Ni/SiC and 20%Ni/Al_2O_3 suffer from deactivation when the integrated test is repeated for multiple cycles, we have examined the stability of the 20%Ni/$MgAl_2O_4$ catalyst. For the 20%Ni/$MgAl_2O_4$ catalyst, the CO conversion is higher for the first cycle (i.e. 88%) than for the second cycle (i.e. 69%) (Fig. 8). This is due to a sintering of the Ni particles after decarbonation at 800 °C. The XRD analysis has shown that after reduction at 600 °C the Ni particles size was less than 2 nm and after further treatment under N_2 at 800 °C for 1 h the Ni particles size increased to 6.8 nm. However, from cycle 2 to cycle 14 significantly less deactivation was observed, as the conversion decreased only from 69% to 61%. The 20%Ni/$MgAl_2O_4$ catalyst appears to be a more suitable catalyst for the integrated CO methanation with CO_2 sorption. One can also note that the sorbent efficiency is not significantly altered as the CH_4 selectivity decreased only from 99% after the first cycle to 96.5% after the 14th cycle.

The rapid deactivation observed for the 20% Ni/SiC catalyst, compared to the 20% Ni/Al_2O_3 and 20% Ni/$MgAl_2O_4$ catalysts, was not expected. In a recent study, Yu et al. [13] have shown that a 15%

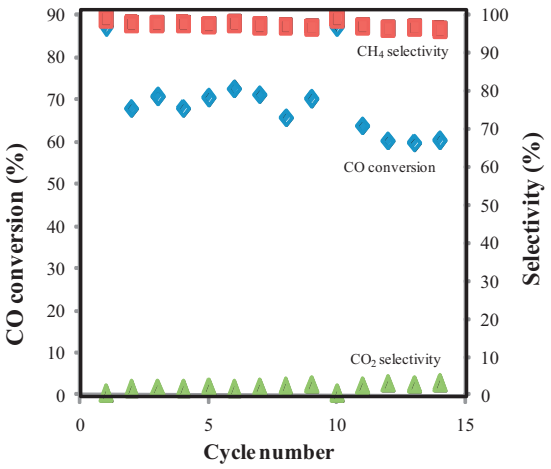

Fig. 8. CO conversion, CH_4 and CO_2 selectivities for each carbonation/decarbonation cycle, for the 20%Ni/$MgAl_2O_4$ catalyst and 68%CaO/$MgAl_2O_4$ sorbent [T = 600 °C, P = 1 atm, GHSV = 22,000 h^{-1}, molar feed composition: H_2 = 38.4%, CO = 38.4%, H_2O = 20%, N_2 = 3.2%; catalyst = 0.1 g, sorbent = 0.7 g].

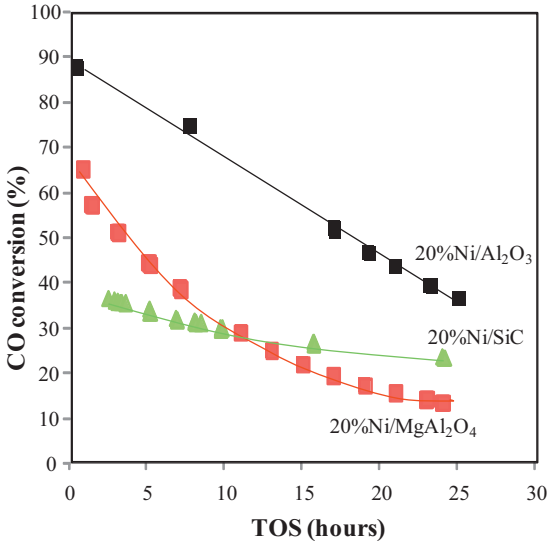

Fig. 9. CO conversion as a function of the time-on-stream for CO methanation reaction for the 20%Ni/SiC (▲), 20%Ni/Al_2O_3 (■) and 20%Ni/$MgAl_2O_4$ (■) catalysts (no sorbent) with T = 500 °C, GHSV = 87,000 h^{-1}, H_2 = 48%, CO = 48% and N_2 = 4%. Catalyst = 0.1 g and SiC diluent = 3.0 g.

Ni/SiC was significantly more stable than a 15% Ni/TiO_2 for the CO methanation at 340 °C and H_2/CO = 3. SiC has excellent thermal conductivity that is supposed to reduce gradients of temperature within catalysts particles and prevent metal particles from sintering that is responsible for deactivation [13]. Since the results of the present study seem to be in disagreement with the literature, we have examined the stability of the three catalysts under conventional CO methanation reaction conditions (i.e. without sorbent and H_2O addition to the feed) and characterized the spent samples to understand the rapid deactivation of the 20% Ni/SiC and 20% Ni/Al_2O_3, compared to the 20% Ni/$MgAl_2O_4$. The results are presented in the following sections.

3.5. CO methanation catalytic performance results

Stability of the 20%Ni/Al_2O_3, 20%Ni/$MgAl_2O_4$ and 20%Ni/SiC catalysts for the CO methanation reaction without sorbent was investigated at 500 °C using a gas mixture of H_2, CO and N_2. Note that H_2O was not added to the gas mixture, in order to mimic the conventional CO methanation reaction. The deactivation is significantly faster when the reaction is conducted at 600 °C without H_2O addition to the feed. Therefore, to better compare the stability of the three catalysts the reaction was conducted at 500 °C. Fig. 9 displays CO conversion as a function of time-on-stream for all three catalysts. 20%Ni/Al_2O_3 and 20%Ni/$MgAl_2O_4$ catalysts exhibited higher initial activity but more rapid deactivation than 20%Ni/SiC catalyst. For example, CO conversion decreased from initial 88% to ~40% (TOS = 25 h) and from initial 65% to ~15% (TOS = 25 h) for the 20%Ni/Al_2O_3 and 20%Ni/$MgAl_2O_4$ catalysts, respectively. On the other hand, 20% Ni/SiC catalyst was more stable and the conversion decreased only from initial ~35% to ~26% (TOS = 25 h). These results are thus in agreement with the stability measurements conducted by Yu et al. [13] showing improved stability when Ni is supported on SiC. To explain the decline in activity and the differences between the three catalysts, both the reduced and spent catalysts were characterized using XRD, TPO-TGA and TEM.

3.6. Characterization of the reduced and spent catalysts

The XRD patterns recorded for the catalysts after reduction and after the CO methanation stability test are displayed in Figs. 10 and 11, respectively. For the reduced catalysts, peaks characteristic of their support (i.e. γAl_2O_3, $MgAl_2O_4$ or βSiC) are present as well as peaks characteristic of Ni° (Fig. 10). No peaks due to NiO phase are present on the XRD patterns. H_2-TPR experiments presented in Fig. 12 show several peaks located between 200 and 900 °C attributed to different type of NiO species having different interaction with the support [24]. The TPR profiles show that after reduction at 600 °C, the 20%Ni/Al_2O_3 and the 20%Ni/SiC catalysts were fully reduced. Note that the peak located at 600 °C for the 20%Ni/SiC catalyst is due to production of methane, from H_2 and carbon impurities of the SiC support, since mass 16 was detected by Mass Spectrometry. For the 20% Ni/$MgAl_2O_4$, the reduction starts at 400 °C and is complete at 800 °C indicating that the nickel was not fully reduced after the reduction treatment at 600 °C. The Ni° particle sizes calculated from the XRD patterns are presented in Table 1. 20%Ni/SiC catalyst contains larger Ni° particles (i.e. 22 nm) likely due to its lower surface area (15 m^2/g) compared to the 20%Ni/Al_2O_3 (122 m^2/g) and 20%Ni/$MgAl_2O_4$ (107 m^2/g) catalysts. Although the 20%Ni/$MgAl_2O_4$ and 20%Ni/Al_2O_3 catalysts have comparable surface area, the Ni° particle size for the 20%Ni/$MgAl_2O_4$ catalyst (4.6 nm) is nearly half that of the size of the Ni° on the 20%Ni/Al_2O_3 catalyst (8.6 nm). Ni° particle sizes of the spent catalysts (i.e. after stability test) were calculated from the XRD patterns presented in Fig. 11. The Ni° particle size of the spent 20%Ni/SiC sample is 22 nm, same as that of the reduced catalyst. This shows that the 20%Ni/SiC catalyst does not sinter during CO

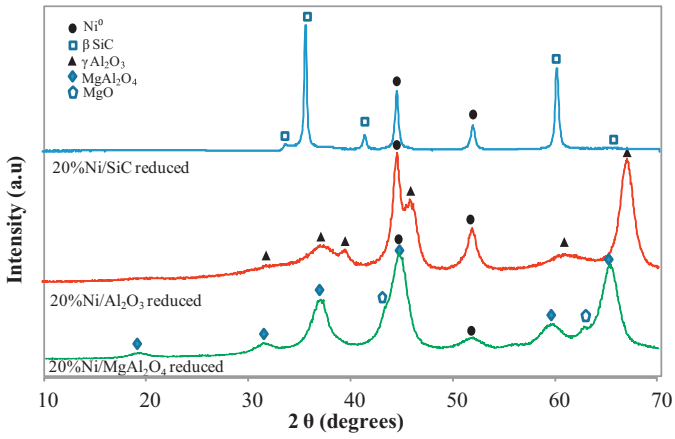

Fig. 10. XRD patterns recorded for the 20%Ni/SiC, 20%Ni/Al_2O_3 and 20%Ni/$MgAl_2O_4$ catalysts after reduction at 600 °C for 2 h under 10% H_2/N_2.

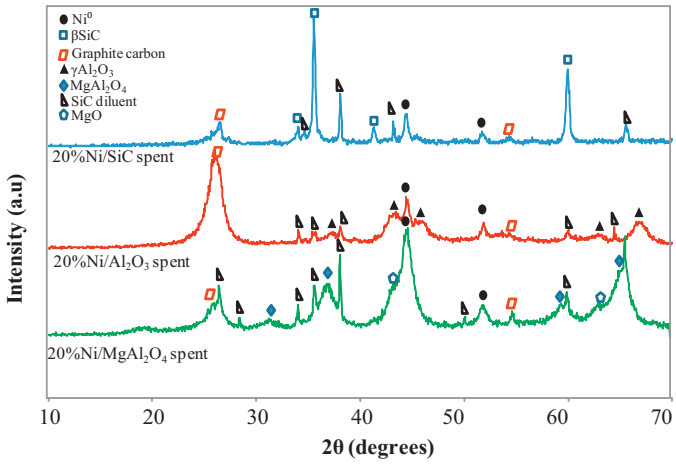

Fig. 11. XRD patterns recorded for the spent 20%Ni/SiC, 20%Ni/Al_2O_3 and 20%Ni/$MgAl_2O_4$ catalysts after stability test for CO methanation.

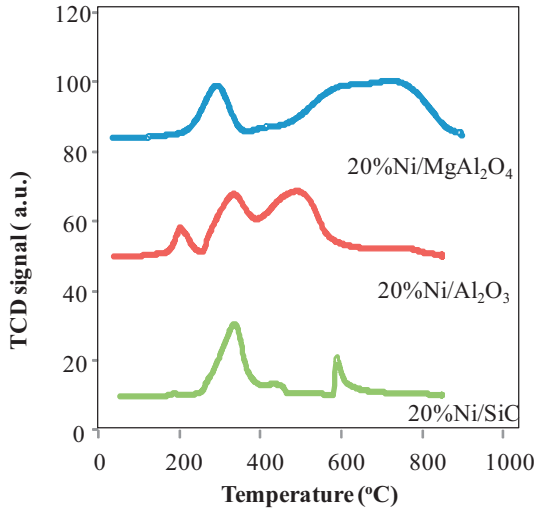

Fig. 12. H_2-TPR profiles for the 20%Ni/SiC, 20%Ni/Al_2O_3 and 20%Ni/$MgAl_2O_4$ catalysts.

methanation. Contrary to the 20%Ni/SiC catalyst, both 20%Ni/Al_2O_3 and 20%Ni/$MgAl_2O_4$ suffer from severe Ni particle sintering during reaction. Specifically, under the methanation reaction conditions tested, Ni° particles size increased from 8.6 nm to 20.6 nm, and from 4.6 nm to 11.2 nm, for the 20%Ni/Al_2O_3 and 20%Ni/$MgAl_2O_4$ catalysts, respectively. Enhanced resistance to Ni particle sintering is one of the major reasons that 20%Ni/SiC is more stable than 20%Ni/Al_2O_3 and 20%Ni/$MgAl_2O_4$ catalysts. The lower conversion observed for the 20%Ni/$MgAl_2O_4$, compared to the 20% Ni/Al_2O_3 presenting a lower Ni dispersion could be due to a potential structure sensitivity [6] or to the basic character of the $MgAl_2O_4$ support as well as the incomplete reduction of the nickel. Acid/base properties of the support have been reported to affect the catalytic activity for the CO methanation and higher CO methanation activity was observed for acidic supports [25,26]. Peaks characteristic of graphite carbon were also detected for all three catalysts using XRD as shown in Fig. 11. The amount of coke present on the spent samples was determined using TPO–TGA analysis. The results shown in Table 1 provide the evidence of a more significant coke formation on the 20%Ni/Al_2O_3 catalyst (69% of coke) compared to the 20%Ni/SiC (25% of coke) and 20%Ni/$MgAl_2O_4$ (31% of coke) catalysts. The higher amount of coke for 20%Ni/Al_2O_3 catalyst, compared to 20%Ni/SiC catalyst, cannot be attributed to the presence of smaller Ni particles (i.e. 8.6 nm vs. 22 nm for 20%Ni/SiC) since

Table 1
BET surface area, Ni particles size and percentage of coke present on the catalysts after stability test for CO methanation (no sorbent included).

Catalyst	Surface area (m^2/g)		Ni° particle size (nm)		Coke (%)
	reduced	spent[a]	reduced	spent[a]	
20%Ni/SiC	15	90	22	22	25
20%Ni/Al_2O_3	122	121	8.6	20.6	69
20%Ni/$MgAl_2O_4$	107	109	4.6	11.2	31

[a] Refers to the catalysts after the stability test, b.

smaller Ni particles are expected to be more resistant to coke formation [27–29]. Higher coke formation for Ni/Al_2O_3 catalyst is likely due to the surface acidity of Al_2O_3. Alkali promoters such as Mg are well known to act as suppressants to retard carbon deposition on methane steam reforming catalysts [30]. Less coking is thus expected for a $MgAl_2O_4$ supported catalyst or a catalyst based on an inert SiC support than for an Al_2O_3 supported catalyst [30]. We can thus conclude that the deactivation observed for the 20%Ni/Al_2O_3 and 20%Ni/$MgAl_2O_4$ catalysts during the stability test measurement was due to the sintering of Ni° particles as well as coking while coking was the main reason for the deactivation of 20%Ni/SiC catalyst.

The spent 20%Ni/SiC, 20%Ni/Al_2O_3 and 20%Ni/$MgAl_2O_4$ catalysts were also analyzed using TEM to determine the nature of coke species. Representative TEM images are shown in Fig. 13. For the spent 20%Ni/Al_2O_3 and 20%Ni/$MgAl_2O_4$ samples, only carbon filaments were observed. For the spent 20%Ni/SiC sample, few carbon filaments were observed with most of the carbon being present in the form of amorphous structures. This has already been observed and attributed to the different interactions between the nickel and the SiC surface, leading to the formation of peculiar exposed nickel faces that are not facile for growing carbon filaments [11]. The presence of amorphous carbon on the spent 20%Ni/SiC also explains the significant increase of its surface area (see Table 1).

It is obvious from these results that the 20% Ni/SiC catalyst is more stable than the 20%Ni/Al_2O_3 and 20%Ni/$MgAl_2O_4$ catalysts under conventional CO methanation reaction conditions due to lower coke formation and less sintering. Hence, the rapid deactivation observed for the 20%Ni/SiC during the cyclic experiments of the integrated test cannot be explained from the stability test results. We have thus analyzed the spent 20%Ni/SiC after the cyclic experiments of the integrated test. The XRD analysis of the spent 20%Ni/SiC sample (after decarbonation and carbonation) revealed the presence of Ni_2Si alloy (inset of Fig. 14). It is likely that the Ni_2Si alloy was formed during the decarbonation step at 800 °C. Indeed,

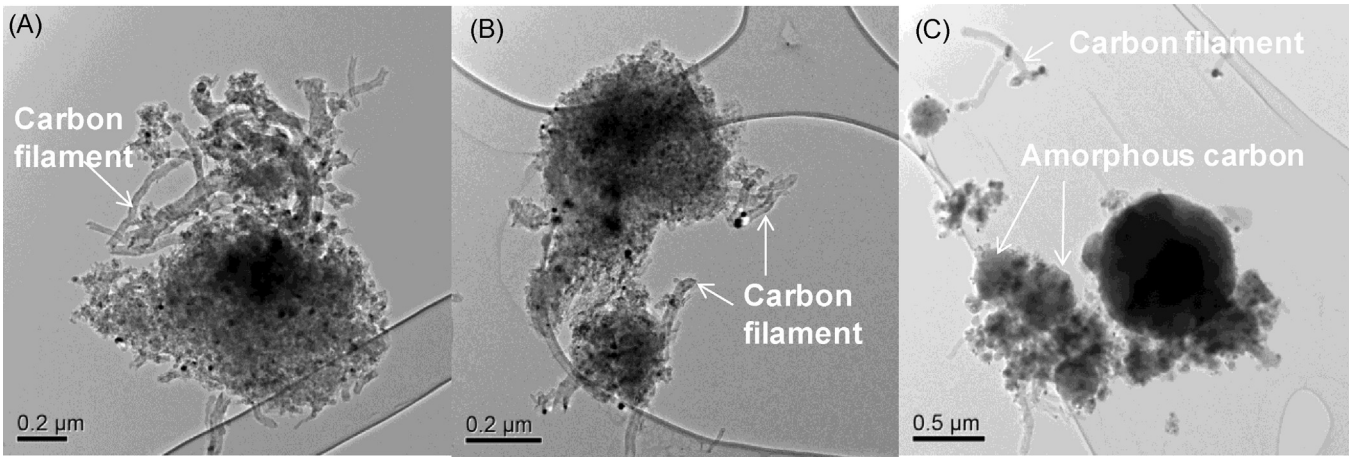

Fig. 13. TEM images for the spent 20%Ni/Al_2O_3 (A), 20%Ni/$MgAl_2O_4$ (B) and 20%Ni/SiC (C).

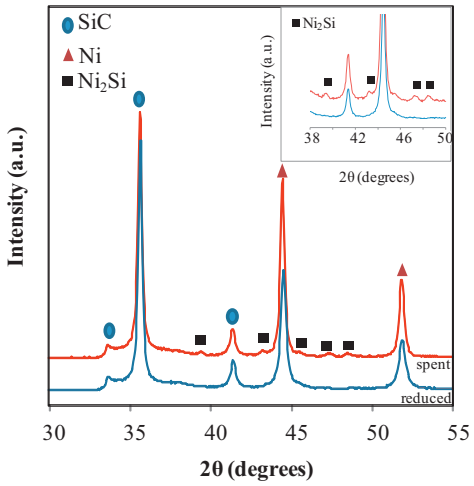

Fig. 14. XRD patterns of the reduced 20%Ni/SiC catalyst and the spent 20%Ni/SiC sample after two carbonation/decarbonation cycles.

an in situ XRD analysis of a Ni/SiC film has shown the formation of Ni_2Si alloy after 4 min at 799 °C under N_2 [31]. According to a study by Imamura and Wallace [32], the activity of Ni_2Si alloy is lower than that of Ni° particles for CO methanation reaction. The formation of Ni_2Si alloy present on the 20%Ni/SiC catalyst could thus be responsible for its deactivation. In addition, Ni° particle size of the spent sample, as determined from the XRD pattern in Fig. 14, also increased to 36 nm compared to that of the reduced catalyst (i.e. 22 nm). This indicates that the Ni particles sinter during the decarbonation step which also contributes to catalyst deactivation. Therefore, the deactivation of 20%Ni/SiC catalyst under the carbonation/decarbonation conditions was due to both sintering of the Ni° particles and transformation of the Ni° particles to Ni_2Si alloy during decarbonation.

Both 20%Ni/Al_2O_3 and 20%Ni/$MgAl_2O_4$ suffer from rapid deactivation under the conventional CO methanation reaction conditions due to sintering and coking. However, the 20%Ni/Al_2O_3 deactivated more quickly than the 20%Ni/$MgAl_2O_4$ during the cyclic experiments, with CO_2 sorption and with steam addition (Figs. 7 and 8). We have thus characterized the spent 20%Ni/Al_2O_3 and 20%Ni/$MgAl_2O_4$ after the cyclic experiments of the integrated test using XRD, and the results are shown in Fig. 15. One can see that the peaks characteristic of the supports are sharper by comparison with the patterns recorded for the reduced catalysts. These results indicate that the degree of crystallization of the Al_2O_3 and $MgAl_2O_4$ supports increased after the multiple carbonation/decarbonation cycles. The high decarbonation temperature (i.e. 800 °C) is likely responsible for the crystallization of the supports. In addition, high decarbonation temperature also caused the sintering of Ni° particles. The Ni° particle size of the spent 20% Ni/$MgAl_2O_4$ increased to 14 nm from 6.8 nm after reduction at 600 °C followed by treatment under N_2 at 800 °C for 1 h. The Ni° particles size is thus twice higher after 20 h on stream. For the 20%Ni/Al_2O_3, under the same conditions the Ni° particles size increased from 10.5 nm to 16 nm. The Ni° particles are thus 1.5 times bigger after only 8 h on stream. We can deduce from these results that the sintering rate is higher for the 20%Ni/Al_2O_3 catalyst during the cyclic experiments. It is also worth noting that coking is more severe for the 20%Ni/Al_2O_3 catalyst than for the 20%Ni/$MgAl_2O_4$ catalyst, as explained above, due to the surface acidity [30]. Hence, the rapid deactivation observed for the 20%Ni/Al_2O_3 compared to the 20%Ni/$MgAl_2O_4$ is likely due to higher coking and sintering rate compared to the 20%Ni/$MgAl_2O_4$.

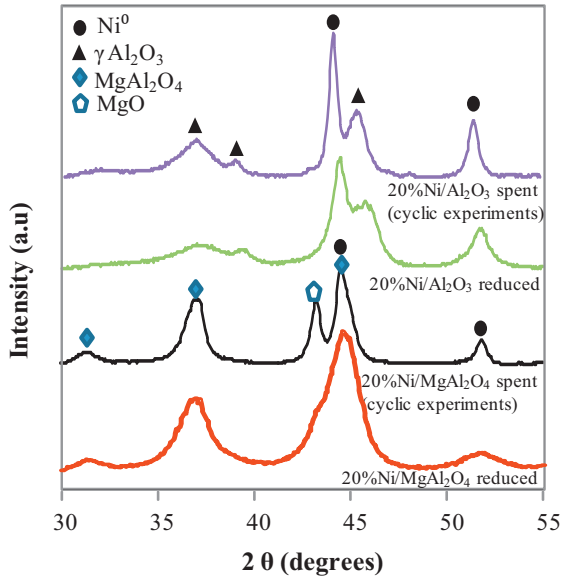

Fig. 15. XRD patterns of for the reduced 20%Ni/Al_2O_3 and 20% Ni/$MgAl_2O_4$ catalysts and for the spent 20%Ni/Al_2O_3 and 20% Ni/$MgAl_2O_4$ samples after multiple carbonation/decarbonation cycles.

4. Conclusion

In this study, we have investigated an integrated process for synthetic natural gas production by combining a CO methanation nickel-based catalyst with a 68%CaO/$MgAl_2O_4$ sorbent. We have shown a significant increase in synthetic methane yield by combining CO methanation, WGS, and CO_2 capture in a single unit, which has a potential application in synthetic natural gas production. The stability of 20%Ni/SiC, 20%Ni/Al_2O_3 and 20%Ni/$MgAl_2O_4$ catalysts when mixed with CO_2 sorbent was studied for multiple carbonation/decarbonation cycles. Both 20%Ni/SiC and 20%Ni/Al_2O_3 showed poor cyclic stability while the 20%Ni/$MgAl_2O_4$ catalyst was found to be more stable in the multiple carbonation/decarbonation studies.

Acknowledgments

The authors gratefully acknowledge financial support for this work provided by the U.S. Department of Energy's Office of Fossil Energy under contract DE-AC-05-76RL01830. We also would like to acknowledge that a portion of this work was done in the Environmental Molecular Sciences Laboratory (EMSL), a DOE sponsored user facility located at PNNL in Richland, WA.

References

[1] International Energy Outlook 2011, http://www.eia.gov/
[2] Y. Ding, W. Han, Q. Chai, S. Yang, W. Shen, Energy & Policy 55 (2013) 445–453.
[3] J. Kopyscinski, T.J. Schildhauer, S.M.A. Biollaz, Fuel 89 (2010) 1763–1783.
[4] D. Harrisson, Industrial & Engineering Chemistry Research 47 (2008) 6486–6501.
[5] H. TopsØe, U.S. Patent 4,130,575 (1978).
[6] J.R. Rostrup-Nielsen, K. Pedersen, J. Sehested, Applied Catalysis A: General 330 (2007) 134–138.
[7] D. Kreuzer, L. Tran-vinh, M. Baerns, Applied Catalysis 15 (1985) 117–126.
[8] K.B. Kester, E. Zagli, J.L. Falconer, Applied Catalysis 22 (1986) 311–319.
[9] S. Therdthianwong, A. Therdthianwong, C. Siangchin, S. Yongprapat, International Journal of Hydrogen Energy 33 (2008) 991–999.
[10] J. Guo, H. Lou, H. Zhao, D. Chai, X. Zheng, Applied Catalysis A: General 273 (2004) 75–82.
[11] P. Leroi, B. Madani, C. Pham-Huu, M.-J. Ledoux, S. Savin-Poncet, J.L. Bousquet, Catalysis Today 91-92 (2004) 53–58.
[12] W.-Z. Sun, G.-Q. Jin, X.-Y. Guo, Catalysis Communications 6 (2005) 135–139.
[13] Y. Yu, G.-Q. Jin, Y.-Y. Wang, X.-Y. Guo, Fuel Processing Technology 92 (2011) 2293–2298.

[14] T. Shimizu, T. Hirama, H. Hosoda, K. Kitano, M. Inagaki, K. Tejima, Chemical Engineering Research and Design 77 (1999) 62–68.
[15] L. Li, D.L. King, Z. Nie, X.S. Li, C. Howard, Energy & Fuels 24 (2010) 3698–3703.
[16] G.S. Grasa, J.C. Abanades, Industrial & Engineering Chemistry Research 45 (2006) 8846–8851.
[17] E.V. Thompson, A Unified Introduction to Chemical Engineering Thermodynamics, Sillwater Press, Orono, ME, 2000, pp. 869–914.
[18] O. Kubaschewski, E.L. Evans, C.B. Alcock (Eds.), Metallurgical Thermochemistry, Pergamon Press Ltd., Oxford, U.K., 1967.
[19] R.W. Hughes, D. Lu, E.J. Anthony, Y. Wu, Industrial & Engineering Chemistry Research 43 (2004) 5529–5539.
[20] V. Manovic, E.J. Anthony, Environmental Science & Technology 41 (2007) 1420–1425.
[21] J.C. Abanades, D. Alvarez, Energy & Fuels 17 (2003) 308–315.
[22] K.O. Albrecht, K.S. Wagenbach, J.A. Satrio, B.H. Shanks, T.D. Wheelock, Industrial & Engineering Chemistry Research 47 (2008) 7841–7848.
[23] Clean Coal Technology Report, available online at www.fe.doe.gov (2000) 1–24.
[24] A. Zhao, W. Ying, H. Zhang, H. Ma, D. Fang, Catalysis Communications 17 (2012) 34–38.
[25] Z. Kowalczyk, K. Stolecki, W. Rarog-Pilecka, E. Miskiewicz, E. Wilczkowska, Z. Karpinski, Applied Catalysis A: General 342 (2008) 35–39.
[26] Q. Xin, X. Shi, P. Ying, X. Guo, Reaction Kinetics and Catalysis Letters 31 (1986) 279–283.
[27] J.-H. Kim, D.J. Suh, T.-J. Park, K.-L. Kim, Applied Catalysis A: General 197 (2000) 191–200.
[28] K.O. Christensen, D. Chen, R. Lodeng, A. Holmen, Applied Catalysis A: General 314 (2006) 9–22.
[29] H. Jeong, K.I. Kim, D. Kim, I.K. Song, Journal of Molecular Catalysis A: Chemical 246 (2006) 43–48.
[30] J.R. Rostrup-Nielsen, Steam Reforming Catalysts, Danish Press, Lingby, 1975, pp. 38–48.
[31] T. Fujimura, S.-I. Tanaka, Journal of Materials Science 34 (1999) 235–239.
[32] H. Imamura, W.E. Wallace, The Journal of Physical Chemistry 83 (1979) 2009–2012.